Volume 6
Number 16
21 August 2025
Pages 5327–5794

Materials Advances

rsc.li/materials-advances

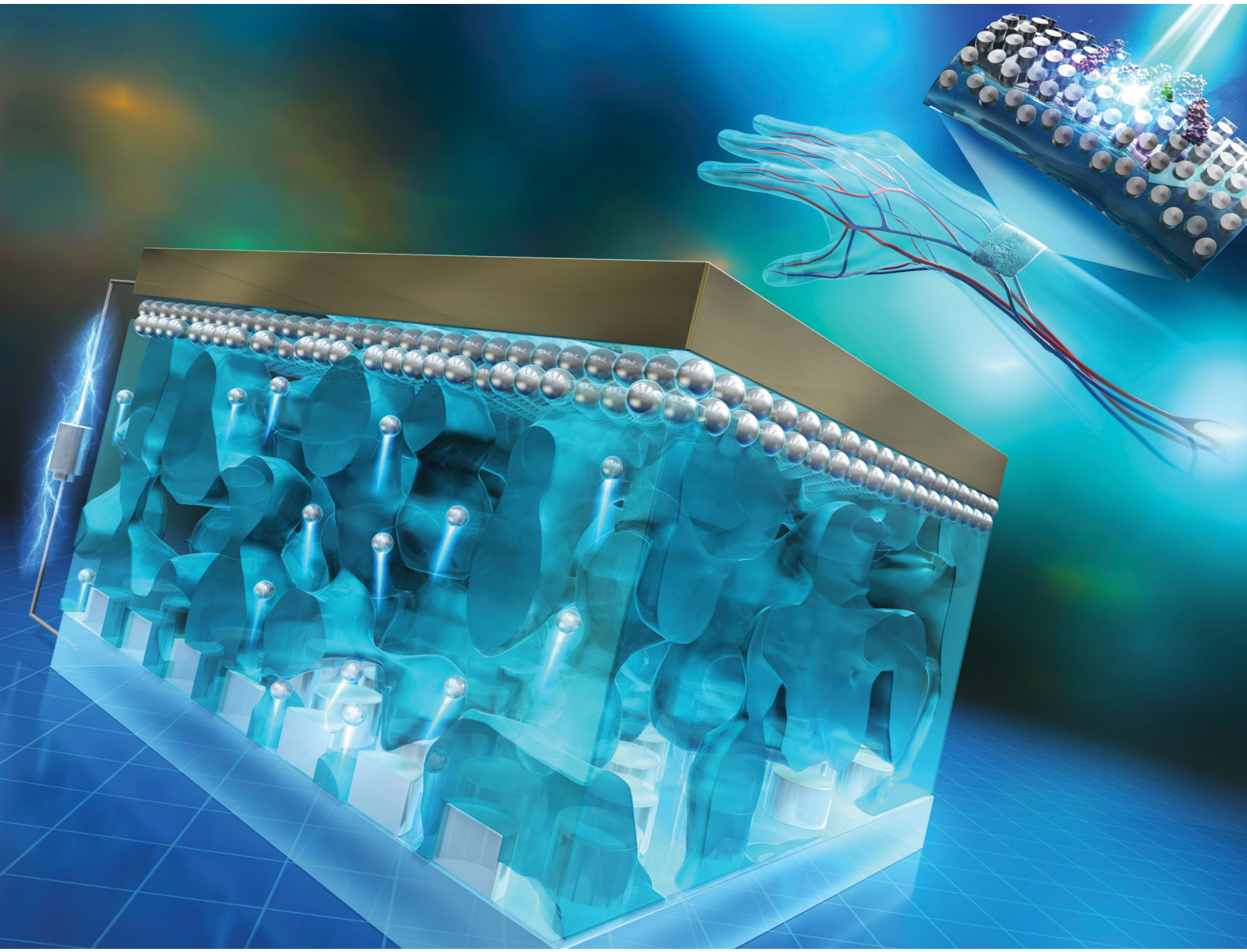

ISSN 2633-5409

ROYAL SOCIETY OF CHEMISTRY

PAPER

Junji Murata *et al.*

Maskless soft lithography for fabricating micro- and nano-scale Ag structures *via* solid-state electrochemical etching using a polymer electrolyte membrane for optoelectronic and sensing applications

Materials Advances

ROYAL SOCIETY OF CHEMISTRY

PAPER

View Article Online
View Journal | View Issue

Cite this: *Mater. Adv.*, 2025, **6**, 5424

Maskless soft lithography for fabricating micro- and nano-scale Ag structures *via* solid-state electrochemical etching using a polymer electrolyte membrane for optoelectronic and sensing applications†

Tatsuya Fujii,[a] Daishi Hakozaki,[a] Atsuki Tsuji,[a] Masaru Takizawa[b] and Junji Murata *[a]

Received 11th March 2025,
Accepted 26th June 2025

DOI: 10.1039/d5ma00218d

rsc.li/materials-advances

Micro/nanostructured Ag surfaces are promising candidates for transparent electroconductive films and highly sensitive plasmonic sensors. However, the conventional patterning procedures are complex and expensive. Here, a direct and simple patterning method is developed *via* solid-state electrolysis using a polymer electrolyte membrane (PEM) stamp. Anodic dissolution of the Ag surface occurs at the PEM/material interface. The Ag ions are transferred through the PEM and deposited as a thin Ag film at the cathode. By optimizing the process conditions, a high etching rate of ~6 μm min^{-1} can be achieved to produce well-defined patterns with resolutions ranging from micrometers to hundreds of nanometers. Multiple processing steps can be combined to generate complex hierarchical structures. This process is performed at room temperature without harsh chemicals and capable of creating Ag patterns on flexible polymer substrates. The resulting patterned surfaces exhibit enhanced optical transmittance, supporting their potential use as flexible electroconductive transparent membranes. The patterned Ag surfaces also enable highly sensitive detection of rhodamine, demonstrating their suitability for surface-enhanced Raman spectroscopy. This fast and facile solid-state electrochemical etching has reduced the environmental impact and cost, making it advantageous for fabricating optoelectronic devices and bio/chemical sensor templates.

1. Introduction

Micro- and nano-structured Ag-based materials have attracted considerable attention owing to their potential applications in flexible electronics, biochemical sensors, and antibacterial surfaces. Ag nanowires and nanoparticles have been widely used for the fabrication of optoelectronic devices such as electroconductive transparent flexible membranes.[1–4] Along with their application in plasmonic sensors, micro- and nano-patterns on Ag surfaces exhibit excellent properties as templates for surface-enhanced Raman spectroscopy (SERS).[5–9] These SERS templates can detect extremely small amounts of toxic chemicals, biomarkers, and illicit drugs. However, complex procedures are required to prepare these templates and flexible electroconductive transparent membranes containing the nanostructured metal surfaces.

Processes to form micro- and nanoscale patterns can be categorized into direct and indirect methods. Photolithography,[10–13] which is essential for semiconductor device fabrication, is the most reliable and common indirect method for producing extremely precise patterns with nanometre resolution. To limit the machined area on the material surface, this method requires a mask (typically a resist film) to protect surface areas that should be preserved. Yet, the use of a resist film makes lithography complex and requires multiple procedures such as spin coating, exposure, development, etching, and ashing, as well as very expensive facilities. Consequently, photolithography incurs a high financial cost and environmental burden. Nanoimprint lithography (NIL) is a direct method for simple and low-cost pattern formation on the material surface without using a resist film. Nevertheless, this approach has been mainly limited to soft polymers, because it is based on plastic deformation to transfer the pattern on the master mold surface to the material surface.

[a] *Department of Mechanical Engineering, Ritsumeikan University, 1-1-1 Noji-Higashi, Kusatsu, Shiga 525-8577, Japan. E-mail: murata-j@fc.ritsumei.ac.jp*
[b] *Department of Physical Sciences, Ritsumeikan University, 1-1-1 Noji-Higashi, Kusatsu, Shiga 525-8577, Japan*

† Electronic supplementary information (ESI) available. See DOI: https://doi.org/10.1039/d5ma00218d

Because the Ag metal is hard with a superior Young's modulus and yield stress, an extremely high pressure is needed to induce its plastic deformation,[14] which can cause material failure. Such a high pressure also shortens the lifespan of the master mold. The fabrication of Ag nanostructures using a superplastic nanomolding technique has been reported.[15,16] However, this approach requires extremely high pressure (~200 MPa) and high temperature (~450 °C) to replicate the mold structure onto the Ag surface. Moreover, repeated use of the Al_2O_3-based mold is not feasible, as the mold must be etched with KOH solution for demolding. Instead of direct NIL based on plastic deformation, there have been extensive reports on forming Ag pattern structures *via* alternative NIL methods by using inks containing Ag nanoparticles or fibers.[17,18] Kim *et al.*[18] developed a soft-contact patterning method: an Ag nanoparticle ink is imprinted using a polydimethylsiloxane (PDMS) stamp, and then the pattern is transferred onto the substrate. Unfortunately, this method is still complex and involves multiple steps. Because the Ag ink contains a solvent, the pattern also has to be baked at ~180 °C for drying, which can induce thermal degradation in polymer substrate materials for flexible devices. Furthermore, the surface morphology of the Ag film depends on the size of particles or fibres in the ink, resulting in a rough surface. Although ink jets or related printing technologies using Ag inks have also been proposed,[19–23] the horizontal resolution achieved by these methods is more than several micrometres, which is inferior to that obtained by lithographic techniques. Another complication originates from the binder in the Ag ink, which covers the Ag nanoparticles and fibres after the solidification process and diminishes the functionality of the Ag nanostructures, such as SERS sensitivity.[5] Laser patterning techniques have also been used to form Ag electrodes.[24–26] However, along with the high power consumption of laser systems, laser irradiation induces intense local heating that could damage flexible polymeric substrates. Laser beam scanning also makes this technology unsuitable for patterning large areas. Colloidal lithography, which uses a monolayer of microspheres as the mask for etching or deposition, can be used to prepare patterned Ag surfaces.[27–29] For example, Bley *et al.*[27] reported a hierarchical Ag pattern comprising micro- and nanohole arrays for use in transparent conductive electrodes. Nevertheless, the colloidal lithographic techniques are multi-step and complex, including the preparation of a microsphere array, plasma treatment to reduce the size of microspheres, reactive ion etching, and metal evaporation. Overall, there remains the need for a direct and simple method to prepare nanostructures on Ag surfaces.

We have developed a new environmentally friendly electrochemical process for fabricating micro- and nanostructures on metal and semiconductor surfaces.[30–35] This process utilizes a solid-phase polymer electrolyte membrane (PEM) as a stamp for imprinting on the material surface, thus allowing electrochemical surface treatment without a liquid electrolyte. Unlike conventional electrochemical etching that involves a liquid electrolyte, in the solid-state method, the electrochemical reactions such as anodic oxidation and dissolution are limited to the contact area between the PEM stamp and material surface. This method is analogous to the conventional NIL process in terms of using a stamp for patterning, but the mechanism of pattern formation is completely different, namely electrochemical reactions instead of plastic deformation of the material. Therefore, the solid-state electrochemical process can directly form nanostructures on hard surfaces such as metals and semiconductors, without employing the resist mask required for the conventional NIL process. Because a solid electrolyte is used instead of the harsh liquid chemicals in direct and one-step patterning, there is no liquid waste for post-treatment or the associated environmental burden.

The solid-state electrochemical process with the PEM stamp can be either anodic oxidation or dissolution, depending on the material to be processed. The oxide pattern, which has a positive structure of the PEM stamp, is formed on Si,[30,33] Ti,[31] and Au[36] surfaces, while anodic dissolution is dominant in producing a nanoscale negative pattern on the Cu surface.[32,35] Considering the presence of sulfonic acid groups in the PEM, the electrochemical reaction proceeds in the contact area between the PEM stamp and material under strongly acidic conditions. This allows us to predict whether oxidation or dissolution is predominant for the treated metals using a pH-potential equilibrium (Pourbaix) diagram.[37] According to the diagram, only Cu among the treated materials can be ionized under acidic conditions, whereas the oxides of Si, Ti, and Au are stable. This diagram also indicates that Ag is soluble in acidic aqueous solutions, suggesting possible direct formation of Ag patterns *via* anodic dissolution at the PEM/Ag interface. Such facile and fast Ag patterning at room temperature without using a resist or harsh liquid chemicals would be advantageous for the fabrication of flexible Ag-based optoelectronic devices and bio/chemical sensors on polymeric substrates.

Herein, we present a green solid-state electrochemical treatment using a PEM stamp to prepare a patterned Ag surface (Fig. 1(a)). The electrochemical reaction at the interface between the PEM stamp and Ag surface was investigated through electrochemical measurements and microscopic elemental analysis. The optimum electrolytic conditions for precise Ag pattern formation were explored. Diverse pattern structures with horizontal resolutions ranging from sub-millimetres to nanometres were successfully formed and investigated using electron and scanning probe microscopy methods. Patterns were also successfully formed in an Ag thin film deposited on the flexible polymer substrate (Fig. 1(b)), and their optical properties were examined with an eye for transparent conductive film applications. Finally, the SERS performance of the patterned Ag surfaces for detecting low-concentration rhodamine molecules was investigated using laser Raman spectroscopy (Fig. 1(d)).

2. Results and discussion

2.1. Ag ionization at the PEM/Ag interface

Electrochemical analysis was performed on the Ag/PEM/Pt electrochemical cell. The linear sweep voltammetry (LSV) profiles (Fig. 2(a-1)) indicate that the wet PEM leads to a much

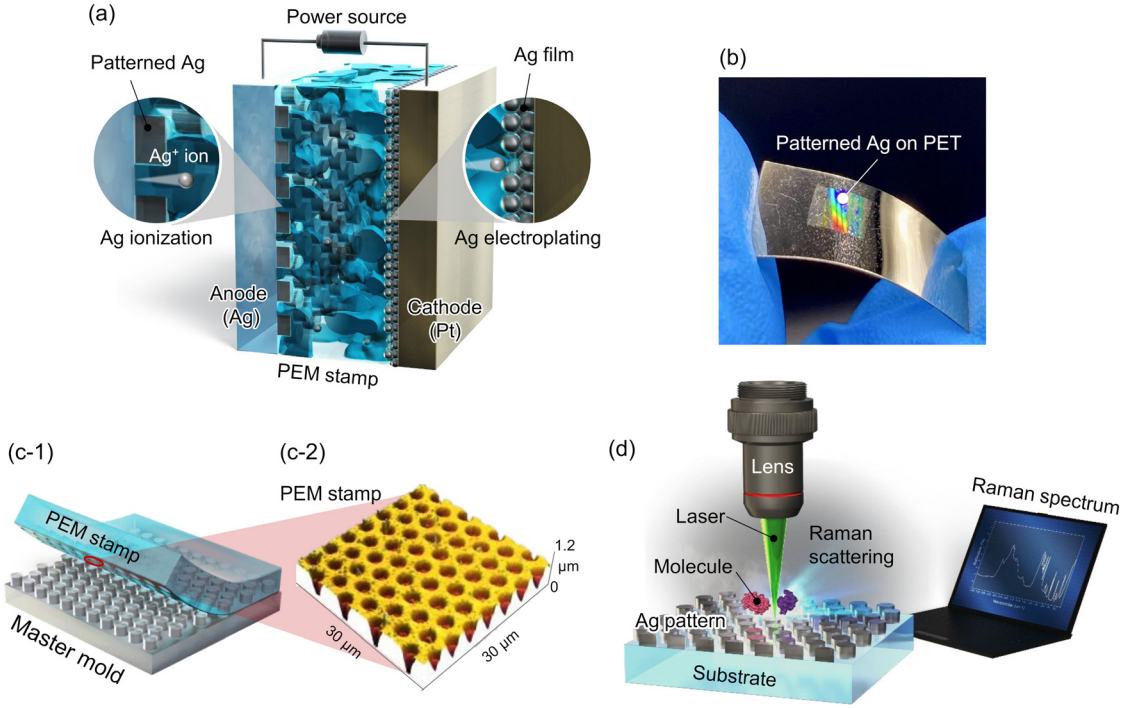

Fig. 1 (a) Schematic of the solid-state electrochemical etching to prepare micro- and nanoscale patterned Ag surfaces. (b) Photograph of a patterned Ag thin film on a flexible PET substrate. (c) Preparation of a PEM stamp. (c-1) Schematic illustration and (c-2) AFM image of the PEM stamp surface. (d) Illustration of applying the patterned Ag surface as a surface-enhanced Raman spectroscopy (SERS) template.

higher current density than the dry PEM, due to the superior ion conductivity of the wet PEM with sufficient nanoscale water channels. The anodic current of the wet PEM begins to increase at a potential of approximately 1 V, and this change can be attributed to the ionization of Ag with a standard electrode potential (E°) of 0.799 V (eqn (1)).

$$Ag(s) \rightarrow Ag^+ + e^- \quad (1)$$

Further increasing the applied potential caused a decrease in the anodic current density, generating a peak at approximately 1.5 V. This indicates that the electrochemical reaction was transformed from a charge transfer-limited process to a diffusion-limited one: a sufficient amount of Ag^+ ions had accumulated in the PEM near the interface with the Ag anode, and their transfer to the cathode limited the electrochemical reaction. An increase in current density was also observed at potentials greater than 2 V, which can be attributed to Ag oxidation (E° = 1.17 V, eqn (2)) and oxygen gas evolution due to water electrolysis (E° = 1.23 V, eqn (3)).

$$2Ag(s) + H_2O \rightarrow Ag_2O(s) + 2H^+ + 2e^- \quad (2)$$

$$2H_2O \rightarrow O_2 + 4H^+ + 4e^- \quad (3)$$

Ag^+ ions that reach the Pt cathode were reduced to form an Ag layer on the cathode (eqn (4)), as illustrated in Fig. 2(a-3).

$$Ag^+ + e^- \rightarrow Ag(s) \quad (4)$$

Alternatively, protons (H^+) generated by oxidation (eqn (2)) or water electrolysis (eqn (3)) can also be reduced at the cathode surface, resulting in hydrogen gas evolution (eqn (5)).

$$2H^+ + 2e^- \rightarrow H_2 \quad (5)$$

A similar trend in the anodic current was observed in the cyclic voltammetry (CV) profiles of the wet PEM with an Ag disk anode, as shown in Fig. 2(a-2). In the negative potential range, a cathodic peak appears at the bias of −1.5 V and can be assigned to the ionization of the Ag film deposited on the Pt electrode (Fig. 2(a-3), right). There is another cathodic peak at around −0.5 V, which should originate from the reduction of Ag oxide (Ag_2O). After replacing the Ag disk electrode with an Ag thin film (thickness ∼100 nm) on the glass substrate as the working electrode, the CV profile changed significantly. As shown in Fig. 2(a-2), the anodic current started to increase at a potential of 0.5 V, a trend that was also observed for the Ag disk anode. However, unlike the case of a thick Ag disk anode, the current suddenly decreased to almost 0 mA cm^{-2} at approximately 1 V, forming a sharp peak. Because the Ag film was very thin (∼100 nm), this rapid drop in electrolytic current density was due to complete removal of the Ag film from the substrate to expose the insulating glass surface, which is evident from the photograph of the Ag/glass sample after measurement (Fig. S3(a), ESI†). These electrochemical measurement results suggest that the Ag surface could be dissolved through solid-state electrolysis at the interface with the wet PEM, when a positive bias greater than 0.5 V is applied.

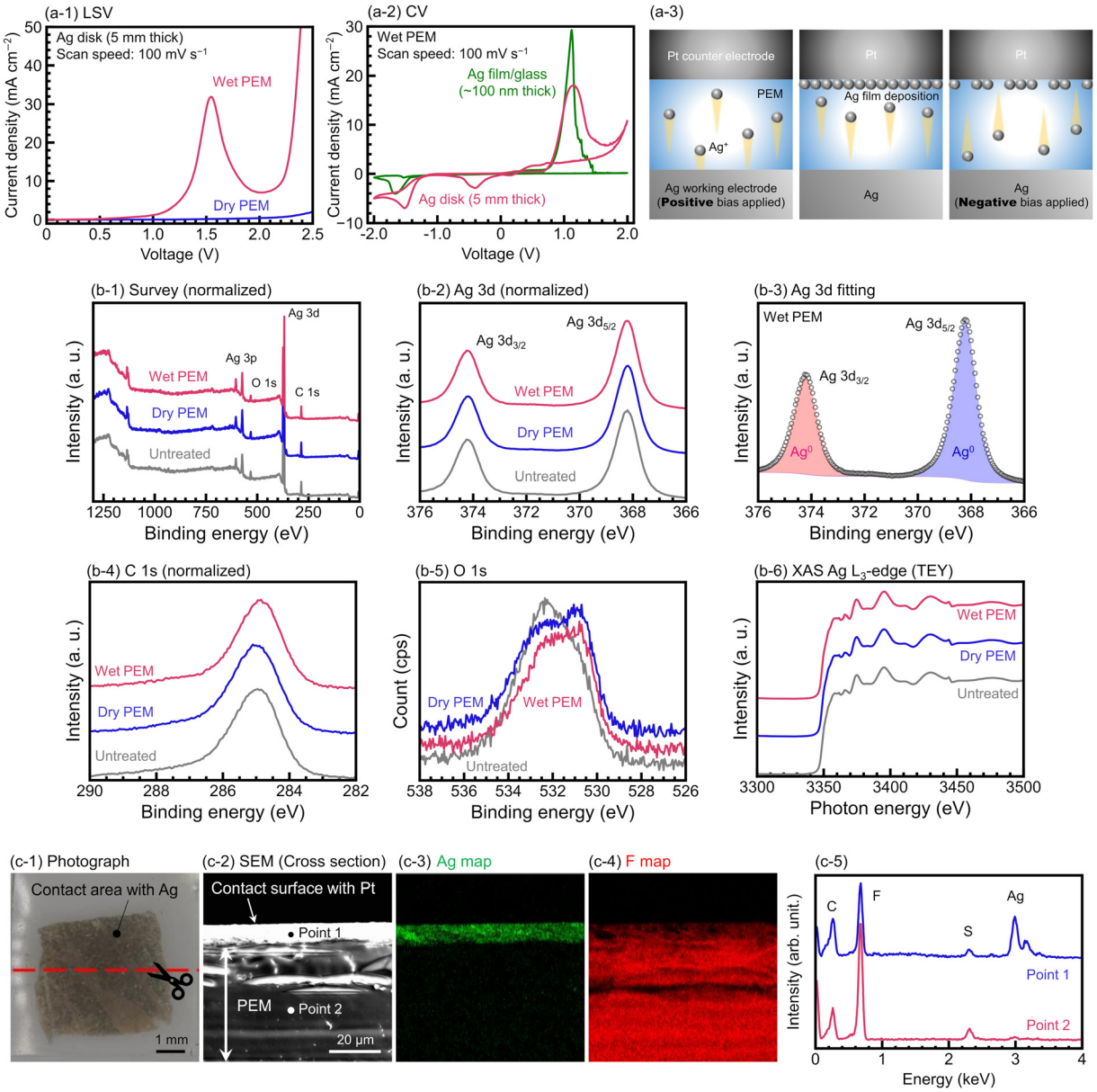

Fig. 2 (a) Electrochemical measurements of the solid-state electrochemical system with pristine (non-patterned) PEM. (a-1) LSV curves obtained using wet and dry PEM. (a-2) CV profiles obtained using the Ag disk (5 mm thick) anode and sputtered Ag thin film (100 nm thick) deposited on the glass substrate as the working electrode. (a-3) Schematic illustration of the electrochemical reaction. From left to right: formation of Ag^+ at the interface between the Ag anode and PEM, deposition of Ag film at the cathode/PEM interface *via* the reduction of Ag^+, and ionization of the deposited Ag film caused by the negative bias. (b) X-ray analysis of Ag surfaces before and after solid-state electrolysis utilizing non-patterned PEM in the wet and dry states. XPS spectra of (b-1) survey scan, (b-2) Ag 3d, (b-3) fitting of Ag 3d (wet PEM), (b-4) C 1s, and (b-5) O 1s. (b-6) XAS Ag L_3-edge total electron yield (TEY) spectra. (c) SEM/EDX analysis of the PEM stamp after solid-state electrolysis. (c-1) A photograph showing the darkened surface area where the stamp contacted the Ag sample. (c-2) Cross-sectional SEM image of the stamp across the darkened area in (c-1). EDX imaging of (c-3) Ag and (c-4) F elements. (c-5) EDX spectra obtained at points 1 and 2 indicated in the SEM image.

The chemical states of the Ag surface after solid-state electrolysis were investigated using X-ray analysis. The X-ray photoelectron spectroscopy (XPS) survey scan (Fig. 2(b-1)) shows Ag 3p, Ag 3d, O 1s, and C 1s peaks both before and after electrolysis. Fig. 2(b-2) displays Ag $3d_{5/2}$ and $3d_{3/2}$ peaks at a binding energy of 368.5 and 374.5 eV, respectively. There was no significant change in the shape of Ag 3d spectra before and after the electrochemical treatment. According to Abe *et al.*,[38] the formation of Ag oxides (AgO or Ag_2O) could cause broader widths in the Ag 3d peaks. However, here the peak width remained almost unchanged after the electrolysis treatment, suggesting that there was no significant Ag oxidation. The peak deconvolution results (Fig. 2(b-3)) reveal that the Ag 3d spectra after electrolysis using the wet PEM can be fitted by two peaks at the binding energies of 368.4 and 374.4 eV, which were assigned to metallic Ag^0 peaks.[38,39] Oxide-related Ag $3d_{5/2}$

components such as Ag^+ and Ag^{2+} (at the binding energy of 367.8 and 367.3, respectively) were not observed in peak fitting. Although our previous study on solid-state electrochemical etching of a Cu surface revealed the formation of a CuO film on the surface treated with the dry PEM,[32] the Ag 3d peak analysis herein clearly suggests the absence of the oxide film on the Ag surface after electrolysis with both dry and wet PEMs. Along with the electrochemical data of the PEM/Ag interface, the Ag 3d XPS spectra provide additional evidence of anodic dissolution of Ag at the interface between the PEM and the material. Furthermore, when Cu and Au surfaces were treated by solid-state electrolysis using the dry PEM, C–F contaminant was formed on the surfaces from the main chain of the PEM (perfluorosulfonic acid, PFSA). Adhesion of this fluorocarbon layer originating from the PEM stamp caused deterioration of the pattern structure, resulting in a short stamp lifetime. However, as shown in Fig. 2(b-1), there was no obvious F 1s peak in the survey scans of Ag surfaces treated by electrolysis, and only a peak related to the hydrocarbon contaminant (C–C or C–H) at a binding energy of 285 eV was observed in the C 1s spectra (Fig. 2(b-4)) without any C–F component (291 eV).[40,41] This suggests that there was no fluorocarbon contaminant caused by adhesion of the PEM component on the Ag surface after solid-state electrolysis, and this can enhance the lifespan of the PEM stamp. As shown in Fig. 2(b-6), the X-ray near edge structure (XANES) Ag L_3-edge spectra exhibited no obvious change in shape after electrolysis. From these X-ray analysis results, we conclude that solid-state electrolysis using the PEM can maintain the chemical state of the Ag surface without introducing contaminant from the PEM component.

Next, the elemental distribution on non-patterned wet PEMs after solid-state electrolysis was investigated using scanning electron microscopy/energy dispersive X-ray spectroscopy (SEM/EDX) analysis. As shown in Fig. 2(c-1), the part of the PEM surface in contact with Ag darkened after electrolysis. The SEM image (Fig. 2(c-2)) and Ag elemental map (Fig. 2(c-3)) clearly demonstrate that Ag was present on the part of the PEM surface in contact with the Pt cathode. Fluorine atoms, which originate from the C–F backbone of the PEM, were almost uniformly distributed inside the PEM (Fig. 2(c-4)). Fig. 2(c-5) shows the EDX spectra taken at two points in the PEM, namely at the interface with the Pt cathode (denoted as "point 1" in the SEM image of Fig. 2(c-2)) and at an interior location ("point 2"). Clear Ag peaks were observed at point 1, and relatively much weaker Ag peaks were observed at the interior point 2. Sulfur peaks derived from the sulfonic acid groups ($-SO_3H$) of the PEM were present at both points. The intensity of the F peak was lower at the interface than that in the interior. The EDX elemental analysis clearly demonstrated that the Ag sample surface was ionized *via* solid-state electrolysis at the interface between the PEM and Ag anode (eqn (1)), and the generated Ag^+ ions were transported from the anode to the cathode through the PEM, driven by the ion concentration gradient. The Ag^+ ions were subsequently reduced at the interface between the PEM and Pt cathode (inverse reaction of eqn (1)) to form a solid Ag thin film on the PEM surface. The results obtained herein provide clear evidence of anodic etching of the Ag surface at the PEM interface. Furthermore, the formation of Ag thin films by reduction at the interface between the PEM and Pt cathode may be a way to electrodeposit Ag thin films without using any liquid electrolyte. Although Akamatsu *et al.*[42,43] reported the solid-state electrodeposition of Cu using a polymer electrolyte membrane, they still employed a liquid electrolyte ($CuSO_4$) to inject Cu^{2+} ions into the PEM, and hence their electrodeposition was performed under quasi-solid state conditions. In contrast, in this study, the solid Ag anode directly supplied Ag^+ ions to the PEM, completely eliminating the use of a plating liquid. In other words, our electroplating method is carried out under fully solid-state conditions, which has not been reported before and can reduce the environmental impact.

2.2. Optimization of electrolytic conditions for precise pattern formation

The effect of bias voltage on the electrochemical etching characteristics was investigated using a PEM stamp with a hole pattern. Fig. 3(a-3) shows the chronoamperometry (CA) profiles recorded at the bias voltages of 1 and 2 V. The electrochemical current density was much higher at 2 V than that at 1 V. In the CA curve at a bias of 2 V, the current density was constant at 200 mA cm^{-2} during the initial stage of electrolysis. At $\sim$0.2 s, however, it rapidly decreased and became almost zero at $\sim$0.4 s. This pattern suggests that after complete Ag removal at the PEM/Ag interface *via* electrochemical etching, the insulating glass surface underneath the Ag thin film was exposed and came in contact with the PEM stamp. The optical microscopy (OM) image of the Ag surface after electrolysis at a bias of 2 V (Fig. 3(a-2)) reveals the formation of a periodic pillar structure on the surface, although there was also an unetched elliptical area. In contrast, a uniform pillar pattern without unetched defects was observed at 1 V. We believe that the large elliptical defect formed at 2 V was due to oxygen gas evolution caused by water electrolysis (eqn (3)) at the PEM/Ag interface. Because the minimum voltage required for water electrolysis is 1.23 V, solid-state electrolysis under the bias of 1 V cannot generate oxygen gas, thus enabling uniform patterning without defects (Fig. 3(a-4), left). In contrast, at 2 V the current flowing through the electrochemical cell was partly used for water electrolysis to generate oxygen gas. The gas bubbles hinder the contact between the PEM and Ag surface (Fig. 3(a-4), right), hence the non-uniform pattern containing defects. These results clearly indicate that electrolysis in the constant-voltage mode should be carried out under a bias below 1.23 V to ensure precise patterning of the material surface.

The effect of etching time on the pattern structure was investigated using a wet PEM stamp containing a 2 μm pillar pattern under a constant bias voltage of 1.2 V. As shown in Fig. S4 (ESI†), the current density rapidly decreased with time as soon as electrolysis started, dropping to almost zero after approximately 3 s. This decrease in current density with time was primarily due to the thinning of the Ag film while etching proceeded. As shown in the SEM images after etching (Fig. 3(b-1)–(b-4)), a clear microhole pattern appeared after a short etching time of 0.1 and 1 s.

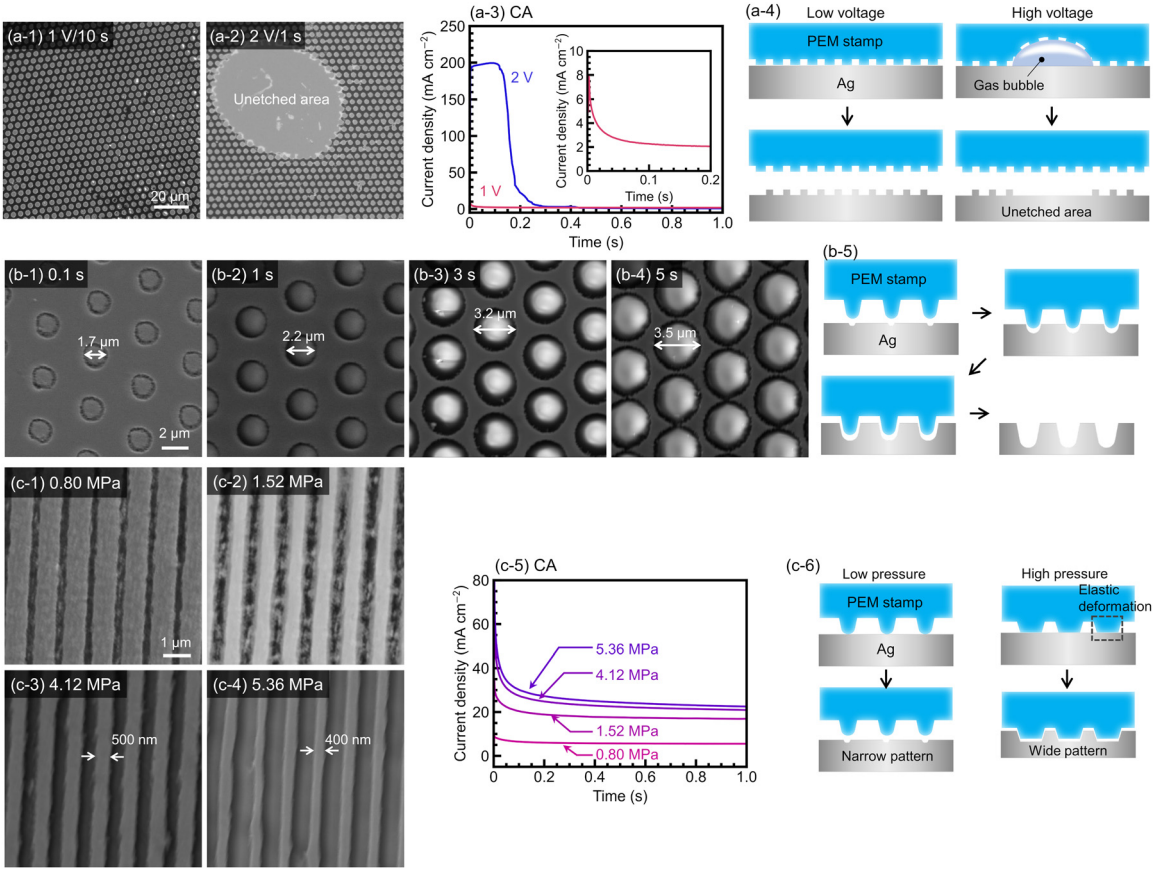

Fig. 3 Effects of different electrochemical conditions on pattern structures formed on Ag surfaces. (a) Effect of the bias voltage applied to the electrochemical cell using the 2 μm hole PEM stamp. OM images of the Ag surface after electrolysis for 1 s under a bias of (a-1) 1 V and (a-2) 2 V. (a-3) CA profiles during electrolysis. (a-4) Schematic of pattern formation under (left) low and (right) high voltage conditions. (b) Effect of electrolytic time using the 2 μm pillar PEM stamp with a bias voltage of 1.2 V and a pressure of 1.52 MPa. SEM images of Ag patterns formed after (b-1) 0.1, (b-2) 1, (b-3) 3, and (b-4) 5 s. (b-5) Schematic of the formation of wider patterns over time. (c) Effect of the contact pressure between the PEM stamp (0.5 μm L&S) and Ag sample. SEM images of patterned Ag surfaces after electrochemical etching under a contact pressure of (c-1) 0.80, (c-2) 1.52, (c-3) 4.12, and (c-4) 5.36 MPa (1 V/1 s). (c-5) CA profiles for different contact pressures. (c-6) Schematic of different pattern widths formed under (left) low and (right) high contact pressures.

Further etching can reduce the pattern accuracy, since the diameter of the holes increased with the etching time. As shown in Fig. S2(b) (ESI†), the pillars on the PEM stamp had a conical structure. In the early stage of etching, only the tips of the pillars were in contact with the Ag surface, forming a hole pattern with a smaller diameter (Fig. 3(b-5)). The contact area increased as etching proceeded, generating larger holes on the Ag surface.

Next, the effect of the contact pressure between the PEM stamp and Ag sample on the pattern structure was investigated. According to the CA profile (Fig. 3(c-5)), the current density at the beginning of electrolysis differed significantly according to the applied contact pressure: the higher the contact pressure, the higher the electrolytic current density. A current density of ~10 mA cm^{-2} was obtained at a pressure of 0.80 MPa, but it became more than five times higher (80 mA cm^{-2}) at 5.36 MPa. In the SEM image of Fig. 3(c-1), narrow grooves were formed on Ag under a pressure of 0.80 MPa. Although an obvious line and space (L&S) pattern was formed on Ag at 1.52 MPa, Ag residues were present inside the formed grooves. Under a low contact pressure, the contact area between the PEM stamp and Ag surface is expected to be small, thereby generating thinner grooves (Fig. 3(c-6), left). Under a higher contact pressure of 4.12 MPa, the etched grooves became wider (500 nm), likely due to the increased contact area between the PEM stamp and Ag surface when the stamp deformed under the applied pressure (Fig. 3(c-6), right). However, at a higher contact pressure of 5.36 MPa, an L&S pattern with narrower lines and a width of ~400 nm was observed on the Ag surface (Fig. 3(c-4)), caused by significant elastic deformation of the PEM stamp. The results described above suggest that highly accurate Ag patterns can be formed by electrochemical etching under the optimal conditions, which in turn depend on the thickness of the Ag film. Considering that the etching time of 1 s is required to remove the Ag film with a thickness of ~100 nm, the etching rate was estimated to be ~6 μm min^{-1}, which offers an extremely high throughput of the patterning process.

2.3. Evaluation of the pattern structures

The surface of Ag thin films on the glass substrate was patterned *via* solid-state electrochemical etching using a PEM stamp. Electrolysis was conducted for 1 s in the constant voltage mode at 1.2 V and a contact pressure of 4.12 MPa using

wet PEM stamps bearing different pattern structures. The morphology and elemental distribution of the treated Ag surfaces were evaluated using SEM and EDX. In Fig. 4(a-1), a precise L&S pattern at a resolution of 2 μm (width of lines) was formed. Although the edges of the Ag lines were partially eroded to produce small indentations, the top surface of the lines exhibited a smooth morphology. Furthermore, the bottom of the grooves appeared smooth. The EDX Ag map shows that Ag was distributed in a striped pattern with clear contrast (Fig. 4(a-2)). In Fig. 4(a-3), Si associated with the SiO_2 glass substrate was mainly observed in the grooves. This suggests that the Ag thin film was almost completely removed by solid-state electrochemical etching, thereby exposing the smooth substrate surface. However, a small amount of Si was widely distributed even in the area of the Ag lines. This is because the Ag film (~100 nm) was thinner than the penetration depth (~0.3 μm) of electrons having an energy of 10 keV.[44] Fig. 4(b) shows the patterned Ag surface formed by treatment using a PEM stamp with a pillar structure, demonstrating that a negative pattern of the PEM stamp was formed on the material surface. The EDX Ag elemental map (Fig. 4(b-2)) reveals that a Ag honeycomb structure was formed on the material surface through solid-state anodic dissolution. According to Fig. 4(c-1), a pillar pattern was formed on the Ag sample under the same electrolytic conditions. The diameter of the pillars (approximately 2 μm) was almost identical to that of the master mold. SEM/EDX analysis of the patterned Ag surfaces demonstrated that the Ag thin film was almost completely removed in the contact area with the PEM stamp. Precise microscale pattern structures could be prepared with an extremely high efficiency (processing time of 1 s) through solid-state electrochemical etching. The atomic force microscopy (AFM) images also confirmed the formation of L&S (Fig. 4(a-4)), hole (Fig. 4(b-4)), and pillar (Fig. 4(c-4)) Ag structures with horizontal resolutions of several microns. Cross-sectional profiles of the surface images revealed that the height of the patterns was approximately 100 nm, matching the Ag film thickness. In Fig. 4(a-4), the line width in the L&S pattern differs slightly along the height of the structure, being 2 μm at the top and 3 μm at the bottom to form trapezoidal cross-sections. A change in the vertical dimension was also observed in the hole pattern (Fig. 4(b-4)). As described earlier in this paper, periodic structures with a non-uniform width were formed on PEM stamps (Fig. S2, ESI†), which were inversely transferred to the material surface. However, the bottoms of the pattern were flat, suggesting that the Ag thin film was completely removed in those areas down to the glass substrate, as discussed in the SEM/EDX analysis of the patterned surface. A comparison of the cross-sectional profiles between the PEM stamps and the resulting Ag patterns (Fig. 4(a-4) and (b-4)) indicates that while pitch accuracy was well preserved, the groove widths of the etched L&S and hole patterns were larger than those of the corresponding PEM structures. This discrepancy is attributed to the elastic deformation of the PEM stamps, particularly in regions with sharp protrusions, as illustrated in Fig. 3(c-6). In contrast, the etched groove width of the pillar pattern (Fig. 4(c-4)) closely matched that of the corresponding PEM structure. The PEM stamp used for pillar patterning (also see Fig. S2(c), ESI†) features wide and flat protrusions, which result in a larger contact area and lower contact pressure between the stamp and the Ag surface. The reduced contact pressure minimizes elastic deformation of the PEM stamp, thereby enabling superior pattern transfer fidelity.

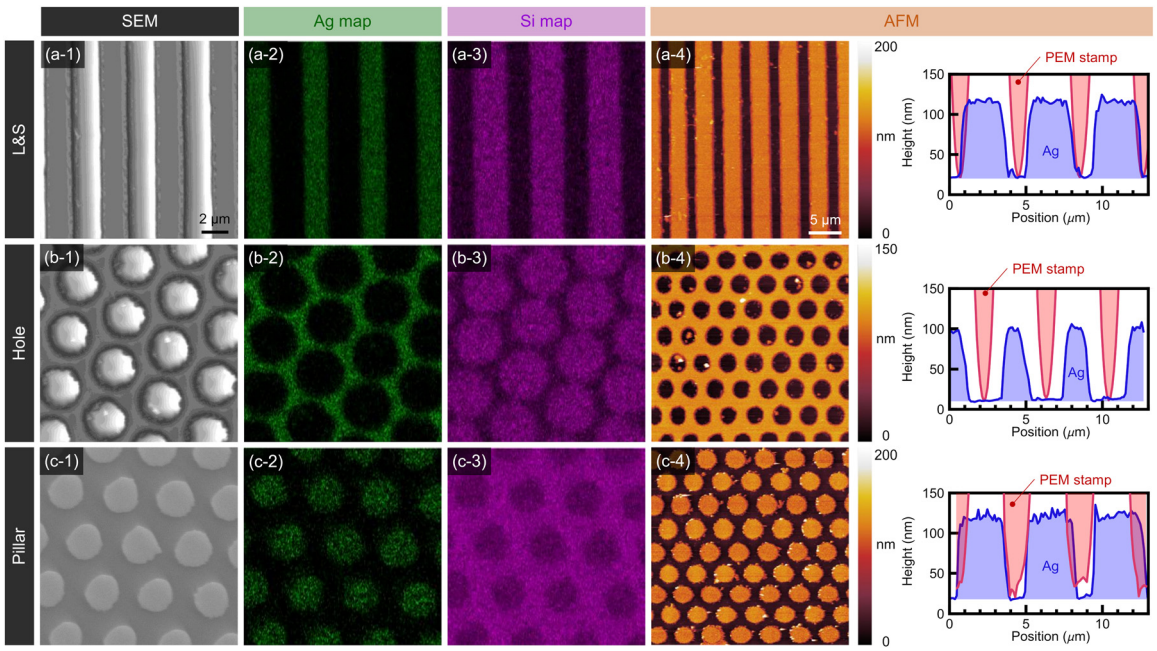

Fig. 4 (a–c) SEM micrographs and EDX elemental analysis of patterned Ag thin films on glass substrates formed *via* solid-state electrochemical etching. Different wet PEM stamps were used to form (a) L&S, (b) hole and (c) pillar structures with a resolution of 2 μm. (1) SEM images. (2) and (3) EDX maps of (2) Ag and (3) Si elements. (4) AFM observation. The cross-sectional profiles of the PEM stamps obtained by AFM are also shown in (4).

Next, we tried to form more precise patterns with a resolution less than 1 μm. Fig. 5(a-1) shows a fine L&S pattern with a resolution of approximately 500 nm formed under the same electrolytic conditions as for the 2 μm pattern (*i.e.*, a bias voltage of 1.2 V and an electrolytic time of 1 s). However, the pattern had poor accuracy, such as a line with non-uniform width and jagged edges. The SEM image of a hole pattern with a diameter of 500 nm (Fig. 5(b-1)) also reveals rough edges and an insufficient etching depth, producing a porous morphology inside the holes. Such rough edges were also observed on the patterned Ag surfaces at 2 μm resolution (Fig. 4), but those jagged edges appear insignificant because their dimensions were smaller compared to the pattern resolution. Conversely, at a finer resolution, rough edges have a more prominent effect on the pattern accuracy. The rough edges on the L&S pattern are likely due to the non-uniform horizontal etching rate, which is attributed to the presence of a thin water layer at the PEM/Ag interface. This water layer, which seeps out from the wet PEM stamp under contact pressure, varies in thickness across the contact area. The local variation in water layer thickness causes corresponding differences in ionic current at the interface, which in turn leads to spatial variation in the horizontal etching rate. This mechanism is considered a key factor contributing to edge instability during electrochemical patterning. The rough edges became more pronounced under conditions of extremely high etching rates. To improve pattern accuracy, we performed electrochemical etching under mild electrolytic conditions with a lower applied voltage of 0.5 V. As shown in Fig. S5 (ESI†), the electrolytic current density at 0.5 V was much lower than that at 1.2 V, and therefore the electrolytic time was extended to 15 s to ensure sufficient etching depth and uniformity. These mild etching conditions resulted in a highly precise L&S pattern with straight edges and a uniform linewidth (Fig. 5(a-2)). The EDX elemental maps for the L&S patterns (Fig. 5(a-3) and (a-4)) demonstrate that a clear elemental distribution was obtained at the lower bias voltage. Furthermore, in Fig. 5(b-2)–(b-4), a well-defined hole pattern with a diameter of approximately 650 nm was obtained under the same conditions. Unlike the hole pattern with porous features obtained at the higher voltage (1.2 V, Fig. 5(b-1)), the holes produced at the lower voltage had a circular shape and smooth edges, forming Ag walls with a width of ∼250 nm between holes. A well-ordered pillar pattern with a diameter of 650 nm was also obtained (Fig. 5(c-2)–(c-4)). The etching rate decreased at a lower electrolytic voltage, leading to more uniform Ag removal at the PEM stamp interface. Uniform etching produces smooth edges when horizontal etching proceeds, resulting in a well-ordered and highly precise pattern. Based on the results obtained herein, suitable electrolytic conditions should be selected by considering the pattern resolution. Note that the etching efficiency was high even under mild electrolytic conditions: a mere processing time of 15 s was required for nanoscale Ag patterning, providing a significant advantage for pattern formation with a resolution ranging from the microscale to nanoscale.

The water contact angle of Ag surfaces was examined. According to Fig. 6(a)–(c), the surfaces with L&S structures exhibit higher contact angles ($>80^\circ$) than the untreated flat surface (54°). The surfaces patterned with hole structures also exhibited a high contact angle of approximately 100°, as shown

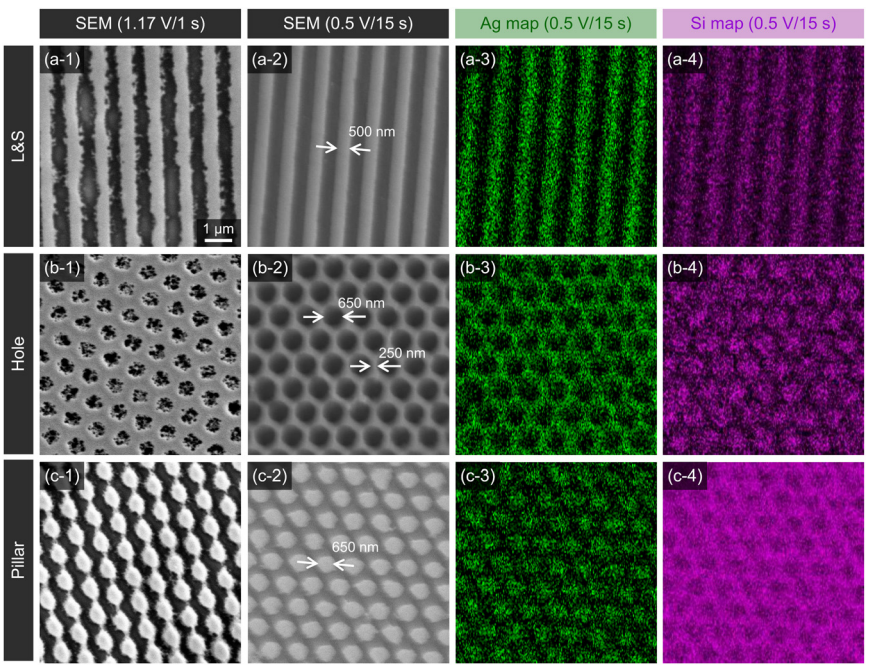

Fig. 5 Optimization of electrolytic conditions to achieve well-ordered nanoscale Ag patterns with a resolution of ∼500 nm consisting of (a) L&S, (b) hole, and (c) pillar structures. SEM images under the electrolytic conditions of (1) 1.2 V for 1 s and (2) 0.5 V for 15 s. EDX maps for (3) Ag and (4) Si elements under the condition of 0.5 V for 15 s.

in Fig. 6(d-1)–(d-3). There is no obvious correlation between the contact angle and pattern resolution (0.5, 1, and 2 μm). The chemical state of the surface affects its wettability such as stronger hydrophilicity (lower contact angle) for the oxidized metal surface as compared to the pristine unoxidized one. However, as described earlier, X-ray analysis of the Ag surface (Fig. 2(b)) revealed no significant change in the chemical composition after solid-state electrolysis treatment. Furthermore, it is evident from the XPS C 1s spectra (Fig. 2(b-4)) that the treated Ag surface was free from fluorocarbon contaminants that could increase the contact angle.[45] Therefore, the significant change in contact angle after pattern formation should be attributed to the surface morphology, as explained by the Wenzel[46] or Cassie's[47,48] law. According to Cassie's theory,[47,48] a surface with a periodic structure has a different contact angle from that of the smooth surface:

$$\cos\theta_c = f(r\cos\theta + 1) - 1$$

where θ_c is the predicted contact angle on the rough surface, f is the projected area ratio of the surface, r is the roughness parameter, and θ is the contact angle on the ideal smooth surface. The SEM and AFM observations confirmed that the L&S pattern contained lines and spaces of almost identical width, hence its projected area ratio is $f = 0.5$. The larger contact angle of the hole pattern may be attributed to its lower f value. When the patterned Ag surfaces are used as a SERS template, the high contact angle on these surfaces may enhance the detection limit due to the condensation effect.[49–51] Furthermore, the hydrophobic nature of the patterned surface can contribute to a high antifouling activity and water resistance when applied to transparent conductive coatings.[52,53]

Now, we try to fabricate even more complex patterns on the Ag surface with different horizontal resolutions ranging from sub-millimeters to nanometers. Fig. 7(a) depicts a Ag patterned surface with periodically arranged squares (size: approximately 300 μm, pitch: 70 μm) formed *via* solid-state electrochemical etching. In this case, the master mold for the PEM stamp was prepared using a blade dicing saw with a 70-μm thick blade on a Si wafer (inset in Fig. 7(a-1)). The scanning white light interferometer (SWLI) image and its cross-section profile (Fig. 7(a-2)) reveal lattice grooves with a depth of ~100 nm and a width of ~70 μm, although some residual Ag film was observed at the bottom of the grooves. We believe that it is possible to further remove this unetched Ag by optimizing the electrolytic conditions. Fig. 7(b) shows a biomimetic surface generated on Ag thin film on glass, with a shark skin-like pattern structure that was reported to have antibacterial properties by inhibiting bacterial adhesion.[54] The PEM stamp was prepared using a commercially available film (Sharklet Shield Panels, Sharklet Technologies, Inc.) as the master mold. A complex pattern comprising microscale trapezoids of different lengths was observed on the surface. The AFM cross-sectional profile (Fig. 7(b-2)) shows that the width of grooves between the trapezoids is less than 1 μm, and the height of the pattern is approximately 100 nm. Although Ag has intrinsic antibacterial properties, the shark skin pattern on the Ag surface can enhance the bactericidal function as reported by Yoo *et al.*[55] Furthermore, Fig. 7(c) demonstrates that two-step solid-state electrochemical etching by applying a single L&S PEM stamp in different directions produced a complex nano-square pattern with a resolution of 500 nm. A hierarchical patterned structure was also formed by using two PEM stamps. Solid-state electrochemical etching was first carried out using one PEM stamp with 2 μm pillar pattern, and further etching was carried out using a second PEM stamp with a finer resolution (0.5 μm) to produce the smaller pattern. The resultant Ag surface, which contained hierarchical hole patterns with two resolutions of 2 and 0.5 μm (Fig. 7(d)), was produced with a total etching time of 2 s. This fast and facile method to form multiscale hierarchical patterns on the Ag surface is very attractive for producing optical devices such as highly sensitive sensors.[56] The height of the patterned structures obtained *via* electrochemical etching was approximately 100 nm, depending on the thickness of the Ag film. However, when a thicker Ag film is used, the achievable pattern depth is believed to be closely related to the height of the PEM stamp. As shown in Fig. S2 (ESI†), the PEM stamps exhibit microscale feature heights ranging from 500 nm to 1 μm, suggesting that deeper Ag etching corresponding to the stamp height can be realized.

As shown in Fig. 8, although the patterned surface morphology varied among different observed points, Ag lines with a width of 100 nm were achieved using the proposed method. Ag droplets were present in the formed lines (Fig. 8(b) and (c)), which are believed to occur through Ag sputter deposition.

The performance of different patterning methods is summarized in Table 1. As previously mentioned, photolithography

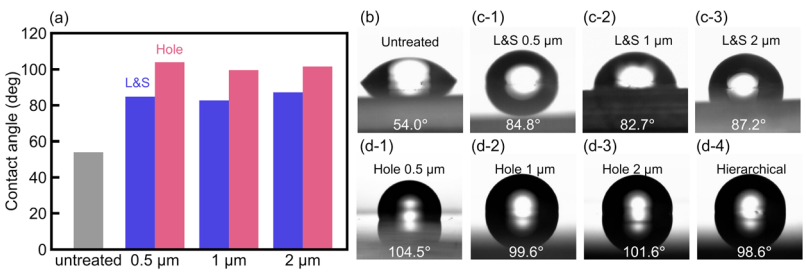

Fig. 6 (a) Water contact angle on untreated and patterned Ag surfaces. Photographs of water droplets on (b) untreated, (c) L&S, and (d) hole patterned Ag surfaces with (1) 0.5 μm, (2) 1 μm, and (2) 0.5 μm resolutions and (d-4) hierarchical hole (2 and 0.5 μm) patterned surfaces.

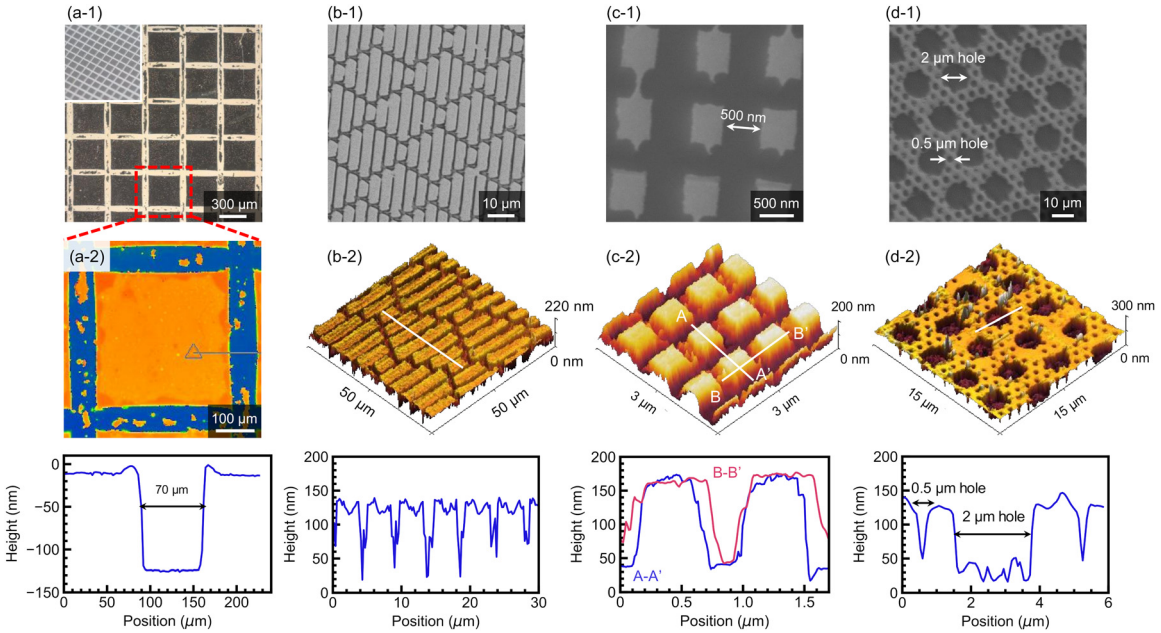

Fig. 7 Formation of diverse Ag patterns with different horizontal resolutions. (a) Sub-millimeter scale square pattern. (a-1) OM image, (a-2) scanning white light interferometer image and cross-sectional profile. The master mold for the PEM stamp was fabricated by forming grooves on a Si wafer using a dicing saw with a 70-μm thick blade. Inset in (a-1): Photograph of the master mold. (b) Microscale complex pattern inspired by shark skin. The PEM stamp was prepared using a commercially available antibacterial film (Sharklet®) as a master mold. (b-1) SEM image, (b-2) AFM observation. (c) Nano-square pattern with a resolution of 500 nm prepared *via* two-step solid-state electrochemical etching using a single L&S PEM stamp. The second electrochemical etching was conducted by rotating the PEM stamp. (c-1) SEM image and (c-2) AFM observation. (d) Hierarchical patterns containing the hole pattern at different resolutions (2 and 0.5 μm) formed by multi-step etching using two different PEM stamps. (d-1) SEM image and (d-2) AFM observation.

is an indirect process that relies on resist coating and involves multiple complex steps. Direct patterning techniques such as UV-NIL, inkjet printing, and laser patterning utilize Ag inks composed of nanowires, nanoparticles, or nanoflakes. However, binders contained in these inks often remain on the surface after patterning, thereby degrading the optical and electrical properties of the Ag nanostructures. Thermal NIL and superplastic nano-molding can directly form patterns on bulk Ag surfaces, but they typically require high temperature and pressure. In contrast, the solid-state electrochemical process employed in this study enables direct formation of nano- and microscale patterns on bulk Ag surfaces without the need for UV exposure, elevated temperature, or high pressure, offering advantages such as low cost, low environmental burden, and process simplicity.

The lifespan and reusability of the PEM stamp are crucial considerations for the industrial application of solid-state electrochemical patterning. As previously discussed, during the electrochemical etching process, Ag ions accumulate within the PEM stamp, leading to Ag film deposition at the interface between the cathode and the PEM (Fig. 2(a-3)). These internalized Ag ions and the deposited film can negatively affect the electrochemical performance of the stamp. In our previous study on solid-state electrochemical etching of Cu, we found that repeated use of the PEM stamp resulted in a reduced etching rate compared to that of a pristine stamp.[35] However, this reduction in etching performance could be recovered by applying a negative bias to the Cu substrate, which was attributed to the electrochemical reduction of Cu ions, thereby lowering their concentration within the PEM. Since the Ag patterning method reported in this study follows a similar mechanism to that used for Cu, we believe that the same recovery treatment—applying a negative bias—would be effective in restoring the PEM stamp's performance in Ag patterning.

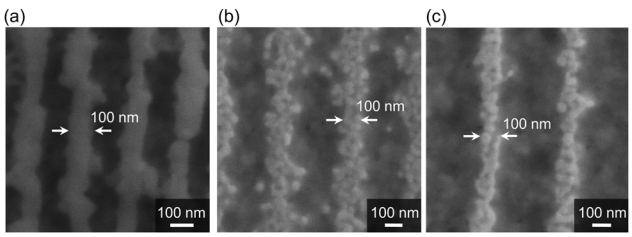

Fig. 8 SEM images of a nanometer-scale L&S pattern with a resolution of 100 nm at three points (a)–(c).

2.4. Optical properties of Ag patterns on flexible substrates

Solid-state electrochemical etching can be performed at room temperature without harsh liquid chemicals, making it suitable for patterning Ag thin films on soft and flexible polymer substrates. Such polymeric substrates are promising for the preparation of flexible optoelectronic devices. Polymer materials such as polyethylene terephthalate (PET) can be easily damaged by high-temperature atmospheres and liquid

Table 1 Comparison of patterning performance

Methods	Direct/indirect	Temperature	Resolution	Comment
Photolithography[10–13]	Indirect	RT	~10 nm	Requires resist and complex steps
UV-NIL[57]	Direct	RT	~100 nm	Uses Ag inks, requires UV exposure
Thermal NIL[15,16]	Direct	~400 °C	~100 nm	Bulk Ag; requires high pressure (~300 MPa)
Inkjet printing[19–23]	Direct	80–100 °C	Several microns	Ag inks; low resolution
Laser patterning[24–26]	Direct	RT	Several microns	Ag inks; localized heating
This work	Direct	RT	~100 nm	Ag film and foil; simple, low-temperature

chemicals. However, the etching method proposed in this study avoided these pitfalls and successfully formed patterns on Ag thin films deposited on PET substrates. As shown in Fig. 9(a), the etching process can achieve L&S patterns on Ag/PET samples with the resolutions of 2, 1, and 0.5 μm. The AFM image in Fig. 9(b-1) confirms an L&S pattern with a line width of ~400 nm and a height of ~100 nm. The top surface of the line (Fig. 9(b-2)) had a smooth micromorphology with a roughness of only 2.50 nm *Sa* (arithmetic average roughness). In contrast, the bottom of the grooves was significantly rougher due to the presence of microparticles with diameters of several hundred micrometers (Fig. 9(b-3)). Such a rough morphology containing microparticles is believed to be due to Ag residue on the bottom, because the untreated PET film has a smooth surface with a roughness of only 1.2 nm *Sa* as observed by AFM (Fig. S6, ESI†). In the photograph of Fig. 1(b), the patterned flexible Ag/PET sample can be easily bent by hand while exhibiting structural rainbow coloration on the patterned area of the Ag film. Optical transmittance spectra were obtained for Ag/PET samples with diverse structures at different resolutions. According to Fig. 9(c-1), the pristine PET film exhibited a transmittance of approximately 90% over the tested wavelength range, whereas the transmittance was only about 10% after Ag film deposition. After etching the Ag film to form patterns, the transmittance increased to 30–50% depending on the pattern structure. As shown in the inset photograph of Fig. 9(c-1), the patterned area is highly transparent to visible light. Fig. 9(c-2) shows that the L&S patterns have almost the same transmittance regardless of the resolution. Electrical resistances for the L&S patterns were measured to be 1.63, 3.30 and 5.83 Ω at resolutions of 2, 1 and 0.5 μm, respectively, which were higher than those for the untreated Ag film deposited on the PET substrate (0.625 Ω). The increased resistance for the smaller resolutions (1 and 0.5 μm) is attributed to the disconnection of the formed lines and the decrease in line width. However, as shown in the inset in Fig. 9(c-2), LED illumination can be achieved using the 1 μm L&S patterned Ag/PET sample integrated into an electrical circuit while being subjected to bending stress. These results demonstrate that fast and facile solid-state electrochemical etching, which is

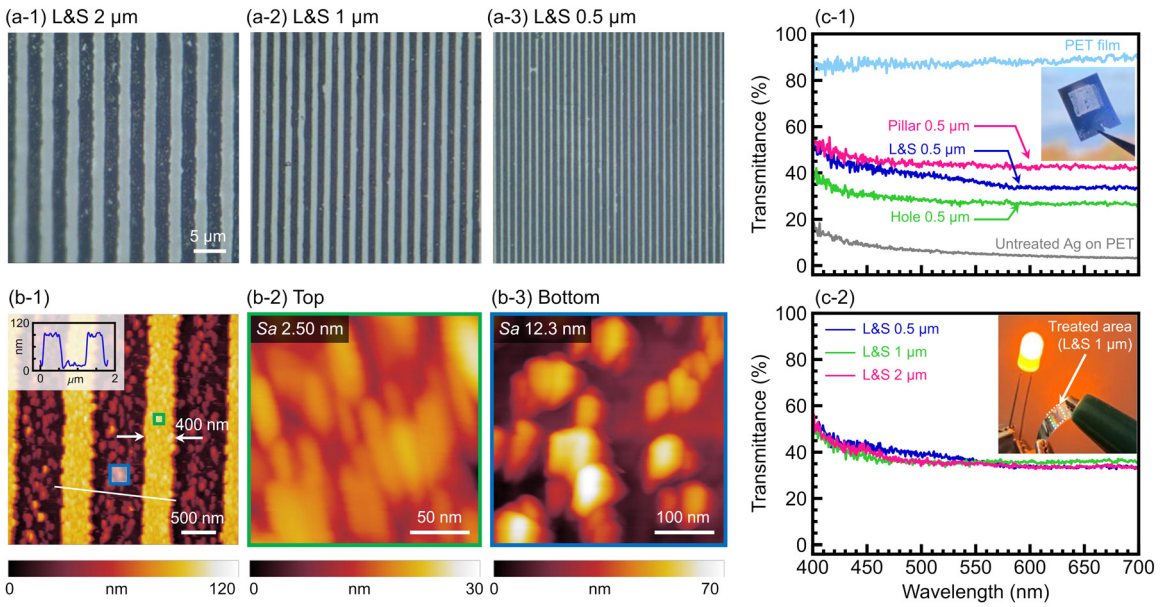

Fig. 9 Pattern formation on an Ag thin film deposited on a flexible PET film *via* solid-state electrochemical etching. (a) OM images of L&S patterns with a resolution of (a-1) 2, (a-2) 1, and (a-3) 0.5 μm. (b) AFM images of patterns on an Ag surface with a resolution of 0.5 μm. (b-1) 3.3 μm × 3.3 μm scan image. Closeup images of (b-2) the top of the pattern (200 nm × 200 nm scan of the area enclosed by green square in (b-1)), and (b-3) the bottom of the pattern (400 nm × 400 nm scan of the area enclosed by blue square in (b-1)). Inset in (b-1): Cross-sectional profile. (c) Optical transmittance spectra of (c-1) Ag films with different pattern structures at the same resolution of 0.5 μm, as well as untreated Ag film and PET film for reference; (c-2) Ag films with L&S patterns at different resolutions. Inset in (c-1) and (c-2): Photographs of the patterned Ag/PET film featuring a hole structure, and a demonstration of an LED circuit based on the 1 μm L&S pattern.

performed at room temperature without using liquid chemicals, can produce flexible optoelectronic devices such as transparent electroconductive membranes.

Finally, the characteristics of patterned Ag surfaces as SERS templates were investigated for detecting rhodamine B (RhB) molecules. Laser Raman spectroscopy analysis was performed for the patterns formed on the Ag foil (50 μm thick) and the Ag/PET template. As shown in Fig. 10(a-1), the untreated Ag surface exhibited no obvious peaks in the spectra, whereas the patterned surfaces with pillar, L&S, and hole structures with a resolution of 0.5 μm showed multiple peaks at wavenumbers around ~1200, 1360, and 1645 cm^{-1}, which are typical signals of RhB on SERS templates.[5–7] Among the patterned structures, the pillar pattern exhibited the highest sensitivity for detecting RhB molecules. The peak intensities for the submicron pillar pattern (0.5 μm resolution) were much higher than those for the microscale patterns (1 and 2 μm), as shown in Fig. 10(a-2). These results suggest that the electromagnetic field was enhanced in the nanogaps between Ag pillars.[49,58,59] The SERS signals of the 0.5 μm pillar pattern depend strongly on the RhB concentration (Fig. 10(a-3)). Although the peak intensity was low, RhB at a concentration of 1 nM (10^{-9} M) can be detected on the patterned Ag surface. The SERS characteristics of the patterned Ag on the flexible PET film were also investigated using a pillar pattern with a resolution of 0.5 μm. Distinct peaks were also observed on the patterned Ag/PET template (Fig. 10(b)), in contrast to the as-deposited Ag film. Micro-Raman imaging for the peak intensity at 1645 cm^{-1} (Fig. 10(c)) was performed. In the optical micrograph (Fig. 10(c-1)), the measurement area included both the patterned and as-deposited flat surfaces. The intensity map (Fig. 10(c-2)) clearly demonstrates that the patterned surface exhibited a higher Raman signal than the as-deposited flat surface. The patterned Ag surface exhibits localized high-intensity areas (“hot spots”) corresponding to the microstructure, which arise from the enhanced electromagnetic field between neighboring Ag features. This non-uniform SERS response, attributed to the pattern resolution (0.5 μm) being larger than the focal laser-spot size (~350 nm) used for the measurements, limits reproducibility across the substrate. Further miniaturization of the pattern resolution—to dimensions smaller than the laser spot—should improve both the uniformity and reproducibility of the SERS signal.

The analytical enhancement factors (EFs) for the different pattern structures were estimated using the following equation:[60]

$$\mathrm{EF} = \frac{I_{\mathrm{SERS}}/C_{\mathrm{SERS}}}{I_{\mathrm{Raman}}/C_{\mathrm{Raman}}} \quad (6)$$

where I_{SERS} and I_{Raman} are intensities of the SERS signal for the patterned Ag surface and normal Raman signal from the patterned Ag surface and the normal Raman signal from the flat Ag surface, respectively, at the wavenumber of 1645 cm^{-1}. C_{SERS} and C_{Raman} are RhB concentrations, both of which are 10^{-3} M. The EFs for the pillar, L&S and hole patterns with 0.5 μm resolution were estimated to be 0.97×10^2, 0.47×10^2,

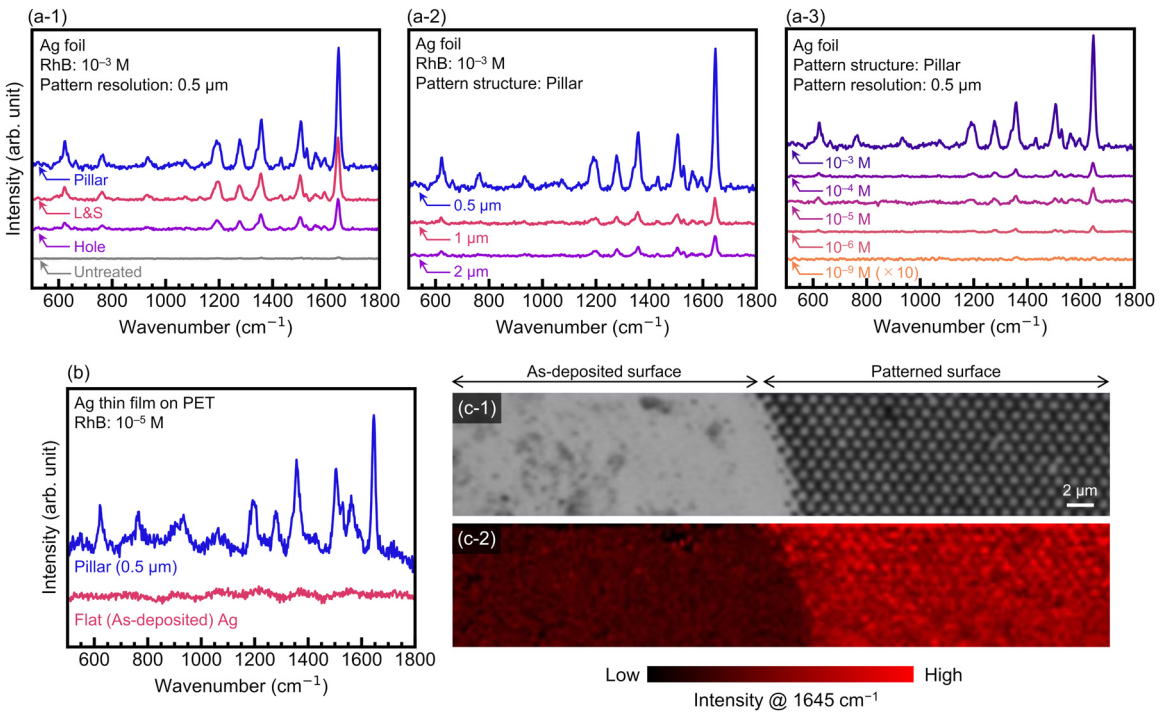

Fig. 10 SERS characteristics of the patterned Ag surface for detecting RhB molecules. (a) Raman spectra for the patterns formed on the Ag foil (50 μm thick): (a-1) effect of the pattern structure (0.5 μm resolution), (a-2) pattern resolution (pillar pattern) and (a-3) RhB concentration. (b) Spectra recorded on the pillar structure with a resolution of 0.5 μm and the as-deposited Ag film on PET. RhB concentration: 10^{-5} M. (c) Raman imaging for the area containing the patterned surface and as-deposited surface: (c-1) optical micrograph and (c-2) intensity map at the wavenumber of 1645 cm^{-1}.

and 0.24×10^2, respectively. Furthermore, when C_{SERS} was 10^{-6} and 10^{-9} M (Fig. 10(a-3)), the EFs for the 0.5 μm pillar pattern were calculated to be 5.1×10^3 and 2.0×10^5, respectively. These results clearly demonstrate that the patterned Ag/PET template enhances the Raman signal for detecting low-concentration RhB molecules. Hence, the proposed solid-state electrochemical etching to form Ag patterns on flexible substrates may be capable of fabricating flexible SERS templates in a fast and facile manner. The Ag nanostructures on the flexible substrate may allow for dynamic and reversible tuning of SERS activity by applying mechanical and thermal strain, as previously demonstrated in temperature-tunable SERS substrates.[61] For broad applications in flexible optoelectronics, large-area preparation of Ag patterns on flexible substrates is essential. In this study, the patterning area was limited by the dimensions of the PEM stamps and was typically 5×5 mm^2. In our previous report on solid-state electrochemical etching of Cu surfaces,[32] a larger patterning area of 50×30 mm^2 was achieved using a roll-to-plate (R2P) system, in which the PEM stamp was adhered to a cylindrical cathode. The R2P system is considered promising for fabricating nanoscale patterned Ag/PET templates over large areas.

3. Conclusions

This study demonstrates a novel method for fabricating micro- and nanostructured Ag surfaces through solid-state electrochemical etching at the interface of a polymer electrolyte membrane (PEM) stamp and an Ag substrate. Electrochemical measurements and SEM/EDX analysis confirmed the occurrence of anodic dissolution of Ag at the PEM/Ag interface, generating Ag^+ ions that migrated through the PEM and were subsequently reduced at the PEM/cathode interface to generate a thin Ag film. Compared to the dry PEM stamp, the wet PEM, produced by soaking the polymer membrane in water, proved to be advantageous owing to its higher ionic conductivity. The applied bias voltage also influenced the resulting pattern. At 2 V, oxygen evolution disrupted uniform etching, whereas well-defined patterns were formed at 1 V. Further optimization of parameters, such as the contact pressure and etching duration, enabled both a high etching rate ($\sim$6 μm min^{-1}) and precise pattern formation. Under the optimized conditions, microscale patterns with resolutions down to 2 μm were achieved. A lower applied electrolytic voltage (0.5 V) allowed patterning on the submicron scale (0.5 μm). Diverse patterns were achieved with the resolution ranging from sub-millimeter to several hundred nanometers. By combining multiple electrolysis steps or multiple PEM stamps, complex patterns such as hierarchical structures were also successfully formed. Because this solid-state electrochemical process operates at room temperature without liquid electrolytes, pattern formation can be achieved on flexible polymer substrates such as PET. The formed Ag pattern/PET samples exhibited a high optical transmittance, indicating their potential as flexible, transparent, and electroconductive membranes. Raman spectroscopy experiments further confirmed that the patterned surfaces served as effective SERS substrates, exhibiting higher sensitivity than the as-deposited flat Ag surface. Reducing the pattern resolution below the laser-spot diameter can significantly enhance the reproducibility of SERS measurements. A more detailed analysis of the effects of Ag pattern structures—such as geometry and resolution—on SERS performance should be conducted in future work.

Future studies should address the durability of the PEM stamps and scale the process to larger areas for industrial applications. Further miniaturization of patterning resolution, while maintaining uniformity remains over a large area, remains a key challenge. Performing the process in a cleanroom environment can further reduce contamination at both the mold/PEM and Ag/PEM interfaces, thereby enhancing patterning uniformity. Nonetheless, this solid-state electrochemical etching method, which is free from harsh chemical solutions and performed under ambient atmospheric conditions, is promising for patterning Ag surfaces in an environmentally benign, cost-effective, and versatile manner. In terms of applications, this approach can be adopted to fabricate advanced flexible devices, transparent conductive membranes, and high-sensitivity SERS templates.

4. Methods

4.1. Sample fabrication

Ag thin films were deposited on optically transparent substrates such as glass and polyethylene terephthalate (PET) films using a magnetron sputtering system (MSP-1S, Vacuum Device Inc.). The typical thickness of the Ag film was approximately 100 nm.

A perfluorosulfonic acid (PFSA) membrane (Nafion N115) with a thickness of 0.125 mm was used to prepare the PEM stamp by thermal imprinting (Fig. 1(c)). Specifically, the as-received Nafion membrane was pressed onto a master mold (DTM-2-1, KYODO International Inc.) at 5 MPa and 135 °C. Prior to the thermal imprinting process, the surfaces of the master mold and PEM film were carefully cleaned by air blowing to remove contaminants such as dust and particulate matter, thereby improving the patterning uniformity of the PEM stamp. After 5 min of pressing, the PEM was naturally cooled to room temperature ($\sim$23 °C) and then detached from the master mold. Owing to the presence of a mold release agent coated on the mold surface, the PEM stamp could be readily detached from the mold without any structural damage. PEM stamps containing three types of pattern structures, namely line and space (L&S), hexagonal close-packed (HCP) hole, and HCP pillar, were prepared on the PEM stamp at different resolutions (0.5–2 μm) and pattern heights (500–1000 nm), as shown in Fig. S2 (ESI†).

Solid-state electrochemical etching was conducted at room temperature under atmospheric pressure. As illustrated in Fig. 1(a), the PEM stamp was sandwiched between the Pt cathode and Ag anode, with the patterned surface of the stamp facing the Ag anode. A desired pressure was applied using a pneumatic cylinder. A liquid electrolyte was not used, and electrolysis was performed in the constant-voltage mode. CA

profiles were obtained during electrolysis using an electrochemical measurement system (potentiostat/galvanostat, HZ-7000, Hokuto Denko Corp.). Afterwards, the PEM stamp was simply removed without further post-etching treatment of the sample surface, such as cleaning.

4.1.1. Characterization. Electrochemical measurements, such as CV and LSV, were performed in a solid-state electrochemical cell comprising a Pt counter electrode, a PEM, and an Ag working electrode, using an electrochemical measurement system and without a reference electrode. Two different Ag working electrodes were compared: a disk Ag electrode (thickness: 5 mm) and a thin Ag film (~100 nm thick) on a glass substrate. The PEM was used in the as-received state without patterning. Electrochemical characteristics of PEM in the dry and wet states were also investigated. The wet PEM was prepared by immersion in deionized water for 10 min, and its water content was estimated to be approximately 10 wt.%. The cross-sectional elemental profile of the PEM after electrolysis was investigated using scanning electron microscopy (SEM; SU6600, Hitachi High-Tech Corp.) with an energy-dispersive X-ray (EDX; INCA-X, Oxford Instruments) system.

The chemical state of the Ag surface after solid-state electrolysis was investigated using synchrotron radiation (SR) X-ray analysis. The Ag surface was treated using wet and dry non-patterned (flat) PEM at a bias voltage of 1 V for 60 s. X-ray photoelectron spectroscopy (XPS) analysis was performed at BL-7 of the Synchrotron Radiation Center (SR-Center), Ritsumeikan University with a 300 W Al Kα X-ray source (1486 eV) under a vacuum pressure of $\sim 7 \times 10^{-8}$ Pa. X-ray absorption spectroscopy (XAS) analysis was performed at BL-13 of the SR-center under a vacuum pressure of $\sim 8 \times 10^{-7}$ Pa. X-ray near-edge structure (XANES) spectra were collected using the total electron yield (TEY) at an evaluation depth of ~50 nm. All X-ray measurements were performed at room temperature.

The patterned structures formed on the Ag surface were observed using optical microscopy (OM; VHX-7000, Keyence), scanning white-light interferometric microscopy (NewView7300, Zygo), and atomic force microscopy (AFM; SPM-9700HT, Shimadzu Corp.). The elemental maps of the patterned Ag surface were obtained using SEM/EDX analysis. The water contact angle on prepared Ag patterns was investigated using a contact angle measurement system (Dropmaster DMC-MC3, Kyowa Interface Science Co., Ltd) with 2-μL droplets of deionized water.

Transmittance spectra of patterned Ag samples on PET film were recorded on a spectrophotometer (PMA-12; Hamamatsu Photonics). To investigate the SERS characteristics of the patterned Ag surfaces on the PET film, Rhodamine B (RhB; R0040, Tokyo Chemical Industry, Inc.) was used as a representative analyte. The patterned Ag surfaces were immersed in a RhB solution for 24 h and then dried in air at room temperature. Raman spectra were collected using a laser Raman microscope (Raman touch VIS-ICS-S, Nanophoton). A laser beam at 532 nm was irradiated on the template surface through a 100× objective lens (NA 0.9) to provide a focal laser spot of approximately 350 nm in size. The spectra were obtained using 600 l mm^{-1} diffractive grating with an irradiation time of 5 s in the wavenumber range of 500–1800 cm^{-1}.

Author contributions

J. M. conceived the study. T. F., D. H. and A. T. designed and conducted the experiments. M. T. performed the X-ray analyses. J. M. authored the manuscript. J. M., D. H., T. F., and A. T. discussed and analyzed the data. All authors read and approved the final manuscript.

Conflicts of interest

There are no conflicts to declare.

Data availability

The data supporting this article have been included as part of the ESI.†

Acknowledgements

This research was partially supported by grants from the JST FOREST Program (Grant Number JPMJFR222P) and JSPS KAKENHI (Grant Numbers 23K17725 and 23H01320).

References

1 Y. Jiang, J. Xi, Z. Wu, H. Dong, Z. Zhao, B. Jiao and X. Hou, *Langmuir*, 2015, **31**, 4950–4957.
2 J. Liang, L. Li, D. Chen, T. Hajagos, Z. Ren, S.-Y. Chou, W. Hu and Q. Pei, *Nat. Commun.*, 2015, **6**, 7647.
3 Y. Chen, R. S. Carmichael and T. B. Carmichael, *ACS Appl. Mater. Interfaces*, 2019, **11**, 31210–31219.
4 Y. Lin, W. Yuan, C. Ding, S. Chen, W. Su, H. Hu, Z. Cui and F. Li, *ACS Appl. Mater. Interfaces*, 2020, **12**, 24074–24085.
5 J. Lee, J. Seo, D. Kim, S. Shin, S. Lee, C. Mahata, H. S. Lee, B. W. Min and T. Lee, *ACS Appl. Mater. Interfaces*, 2014, **6**, 9053–9060.
6 S. Lin, W.-L.-J. Hasi, X. Lin, S. Han, X.-T. Lou, F. Yang, D.-Y. Lin and Z.-W. Lu, *Anal. Methods*, 2015, **7**, 5289–5294.
7 S. Mao, F. Pei, S. Feng, Q. Hao, P. Zhang, Z. Tong, X. Mu, W. Lei and B. Liu, *Colloids Surf., A*, 2023, **657**, 130595.
8 Y. Lu, X. Zhang, L. Zhao, H. Liu, M. Yan, X. Zhang, K. Mochizuki and S. Yang, *Nat. Commun.*, 2023, **14**, 5860.
9 J. Li, Y. Feng, L. Liang, F. Liao, W. Huang, K. Li, G. Cui and Z. Zuo, *ACS Appl. Mater. Interfaces*, 2024, **16**, 35771–35780.
10 J. Wang, J. Jiu, T. Sugahara, S. Nagao, M. Nogi, H. Koga, P. He, K. Suganuma and H. Uchida, *ACS Appl. Mater. Interfaces*, 2015, **7**, 23297–23304.
11 Y. U. Kim, N. Y. Kwon, S. H. Park, C. W. Kim, H. D. Chau, M. H. Hoang, M. J. Cho and D. H. Choi, *ACS Appl. Mater. Interfaces*, 2021, **13**, 61463–61472.
12 G. S. Liu, T. Wang, Y. Wang, H. Zheng, Y. Chen, Z. Zeng, L. Chen, Y. Chen, B. R. Yang, Y. Luo and Z. Chen, *Nano Res.*, 2022, **15**, 2582–2591.
13 T. Okabe, J. Tang, K. Nishimura and N. Shikazono, *Nanomaterials*, 2023, **13**, 3035.

14 W. I. Park, T. W. Park, Y. J. Choi, S. Lee, S. Ryu, X. Liang and Y. S. Jung, *ACS Nano*, 2021, **15**, 10464–10471.
15 J. Xiang, Y. Wang, Y. Wu, H. Fang, L. Shui, Z. Liu and T. Ding, *ACS Appl. Nano Mater.*, 2021, **4**, 11644–11650.
16 J. Xiang, Y. Wang, Y. Wu, Q. Peng, L. Shui, W. Ouyang, T. Ding and Z. Liu, *Adv. Mater. Technol.*, 2022, **7**, 1–7.
17 F. McGrath, J. Qian, K. Gwynne, C. Kumah, D. Daly, C. Hrelescu, X. Zhang, D. M. O'Carroll and A. Louise Bradley, *Appl. Surf. Sci.*, 2021, **537**, 147892.
18 M. Kim, D. K. Oh, J. D. Kim, M. Jeong, H. Kim, C. Jung, J. Song, W. Lee, J. Rho and J. G. Ok, *Nanophotonics*, 2022, **11**, 2693–2700.
19 N. Zhang, J. Luo, R. Liu and X. Liu, *RSC Adv.*, 2016, **6**, 83720–83729.
20 W. Zhang, E. Bi, M. Li and L. Gao, *Colloids Surf., A*, 2016, **490**, 232–240.
21 J. Kastner, T. Faury, H. M. Außerhuber, T. Obermüller, H. Leichtfried, M. J. Haslinger, E. Liftinger, J. Innerlohinger, I. Gnatiuk, D. Holzinger and T. Lederer, *Microelectron. Eng.*, 2017, **176**, 84–88.
22 Q. Huang, K. N. Al-Milaji and H. Zhao, *ACS Appl. Nano Mater.*, 2018, **1**, 4528–4536.
23 N. Karim, S. Afroj, S. Tan, K. S. Novoselov and S. G. Yeates, *Sci. Rep.*, 2019, **9**, 1–10.
24 J. W. Yoon, W. S. Chang and S. H. Cho, *Opt. Lasers Eng.*, 2015, **73**, 40–45.
25 S. Y. Ji, C. M. Ajmal, T. Kim, W. S. Chang and S. Baik, *Nanotechnology*, 2017, **28**, 165301.
26 X. Luo, W. Liu, C. Chen, G. Jiang, X. Hu, H. Zhang and M. Zhong, *Opt. Laser Technol.*, 2021, **139**, 106969.
27 K. Bley, J. Semmler, M. Rey, C. Zhao, N. Martic, R. N. Klupp Taylor, M. Stingl and N. Vogel, *Adv. Funct. Mater.*, 2018, **28**, 1706965.
28 A. E. Kandjani, R. Ramanathan, M. Zabara, Y. M. Sabri, S. K. Bhargava and V. Bansal, *Small Methods*, 2019, **3**, 1–9.
29 R. Kaneko, H. Ichikawa, M. Hosaka, Y. Sone, Y. Imura, K. H. Wang and T. Kawai, *Langmuir*, 2022, **38**, 8153–8159.
30 R. Umezaki and J. Murata, *Mater. Chem. Phys.*, 2021, **259**, 124081.
31 P. Jia, R. Umezaki and J. Murata, *Microelectron. Eng.*, 2022, **257**, 111752.
32 A. Tsuji, E. Morimoto, M. Takizawa and J. Murata, *Adv. Mater. Interfaces*, 2024, **11**, 2300896.
33 K. Yamazaki, A. Tsuji, M. Takizawa and J. Murata, *Small Methods*, 2024, **2301787**, 1–11.
34 T. Fujii, A. Tsuji, M. Takizawa and J. Murata, *Nanoscale*, 2024, **16**, 18811–18823.
35 A. Tsuji, T. Kobayashi and J. Murata, *ACS Appl. Mater. Interfaces*, 2025, **17**, 21929–21939.
36 T. Fujii, A. Tsuji, M. Takizawa and J. Murata, *Nanoscale*, 2024, **16**, 18811–18823.
37 M. Pourbaix and J. A. Franklin, *Atlas of electrochemical equilibria in aqueous solutions*, National Association of Corrosion Engineers, 1974.
38 Y. Abe, T. Hasegawa, M. Kawamura and K. Sasaki, *Vacuum*, 2004, **76**, 1–6.
39 D. Lützenkirchen-Hecht and H. H. Strehblow, *Surf. Interface Anal.*, 2009, **41**, 820–829.
40 F. Y. Zhang, S. G. Advani, A. K. Prasad, M. E. Boggs, S. P. Sullivan and T. P. Beebe, *Electrochim. Acta*, 2009, **54**, 4025–4030.
41 B. Avasarala, R. Moore and P. Haldar, *Electrochim. Acta*, 2010, **55**, 4765–4771.
42 K. Akamatsu, S. Nakano, K. Kimura, Y. Takashima, T. Tsuruoka, H. Nawafune, Y. Sato, J. Murai and H. Yanagimoto, *ACS Appl. Mater. Interfaces*, 2021, **13**, 13896–13906.
43 S. Yamada, Y. Takashima, T. Tsuruoka and K. Akamatsu, *RSC Appl. Interfaces*, 2024, **1**, 1069–1076.
44 K. Kanaya and S. Okayama, *J. Phys. D: Appl. Phys.*, 1972, **5**, 43.
45 S. A. Kulinich and M. Farzaneh, *Vacuum*, 2005, **79**, 255–264.
46 R. N. Wenzel, *J. Phys. Colloid Chem.*, 1949, **53**, 1466–1467.
47 A. B. D. Cassie and S. Baxter, *Nature*, 1945, **155**, 21–22.
48 A. J. B. Milne and A. Amirfazli, *Adv. Colloid Interface Sci.*, 2012, **170**, 48–55.
49 Z. X. Yan, Y. L. Zhang, W. Wang, X. Y. Fu, H. B. Jiang, Y. Q. Liu, P. Verma, S. Kawata and H. B. Sun, *ACS Appl. Mater. Interfaces*, 2015, **7**, 27059–27065.
50 L. Xiao, M. Zhang, Z. Liu, W. Bian, X. Zhang and J. Zhan, *Anal. Methods*, 2017, **9**, 1816–1824.
51 W. A. Tegegne, W. N. Su, A. B. Beyene, W. H. Huang, M. C. Tsai and B. J. Hwang, *Microchem. J.*, 2021, **168**, 106349.
52 B. Zhou, Z. Li, Y. Li, X. Liu, J. Ma, Y. Feng, D. Zhang, C. He, C. Liu and C. Shen, *Compos. Sci. Technol.*, 2021, **201**, 108531.
53 I. Torun, N. Celik, N. B. Kiremitler, X. Huang and M. S. Onses, *Surf. Interfaces*, 2023, **36**, 102576.
54 M. L. Carman, T. G. Estes, A. W. Feinberg, J. F. Schumacher, W. Wilkerson, L. H. Wilson, M. E. Callow, J. A. Callow and A. B. Brennan, *Biofouling*, 2006, **22**, 11–21.
55 C. H. Yoo, Y. Jo, J. H. Shin, S. Jung, J.-G. Na, T. Kang and J. S. Lee, *Chem. Eng. J.*, 2022, **432**, 134363.
56 R. Peng, T. Zhang, S. Wang, Z. Liu, P. Pan, X. Xu, Y. Song, X. Liu, S. Yan and J. Wang, *Anal. Chem.*, 2024, **96**, 10620–10629.
57 H. Zhou, H. Mao, X. Meng, Q. Wang, L. Tan and Y. Chen, *Org. Electron.*, 2019, **75**, 105408.
58 J. Cai, C. Lv and A. Watanabe, *ACS Appl. Mater. Interfaces*, 2015, **7**, 18697–18706.
59 J. Lu, J. Yang, S. C. Singh, Z. Zhan, Z. Yu, W. Xin, T. Huang and C. Guo, *Appl. Surf. Sci.*, 2019, **478**, 737–743.
60 E. C. Le Ru, E. Blackie, M. Meyer and P. G. Etchegoint, *J. Phys. Chem. C*, 2007, **111**, 13794–13803.
61 F. Deng, J. Xiang, S. Wang, X. Wang, H. Hu, Z. Liu and T. Ding, *Adv. Mater. Interfaces*, 2022, **9**, 1–6.